Cerebrovascular disease in patients with COVID-19: neuroimaging, histological and clinical description

Francisco Hernández-Fernández,[1] Hernán Sandoval Valencia,[2] Rosa Angélica Barbella-Aponte,[3] Rosa Collado-Jiménez,[4] Óscar Ayo-Martín,[1] Cristina Barrena,[2] Juan David Molina-Nuevo,[4] Jorge García-García,[1] Elena Lozano-Setién,[4] Cristian Alcahut-Rodriguez,[1] Álvaro Martínez-Martín,[1] Antonio Sánchez-López[5] and Tomás Segura[1]

Abstract

Since the appearance of the first case of coronavirus disease 2019 (COVID-19) a pandemic has emerged affecting millions of people worldwide. Although the main clinical manifestations are respiratory, an increase in neurological conditions, specifically acute cerebrovascular disease, has been detected. We present cerebrovascular disease case incidence in hospitalized patients with SARS-CoV-2 infection. Patients were confirmed by microbiological/serological testing, or on chest CT semiology. Available data on comorbidity, laboratory parameters, treatment administered, neuroimaging, neuropathological studies and clinical evolution during hospitalization, measured by the modified Rankin scale, were analysed. A bivariate study was also designed to identify differences between ischaemic and haemorrhagic subtypes. A statistical model of binary logistic regression and sensitivity analysis was designed to study the influence of independent variables over prognosis. In our centre, there were 1683 admissions of patients with COVID-19 over 50 days, of which 23 (1.4%) developed cerebrovascular disease. Within this group of patients, cerebral and chest CT scans were performed in all cases, and MRI in six (26.1%). Histological samples were obtained in 6/23 cases (two brain biopsies, and four arterial thrombi). Seventeen patients were classified as cerebral ischaemia (73.9%, with two arterial dissections), five as intracerebral haemorrhage (21.7%), and one leukoencephalopathy of posterior reversible encephalopathy type. Haemorrhagic patients had higher ferritin levels at the time of stroke (1554.3 versus 519.2, P = 0.004). Ischaemic strokes were unexpectedly frequent in the vertebrobasilar territory (6/17, 35.3%). In the haemorrhagic group, a

characteristic radiological pattern was identified showing subarachnoid haemorrhage, parieto-occipital leukoencephalopathy, microbleeds and single or multiple focal haematomas. Brain biopsies performed showed signs of thrombotic microangiopathy and endothelial injury, with no evidence of vasculitis or necrotizing encephalitis. The functional prognosis during the hospital period was unfavourable in 73.9% (17/23 modified Rankin scale 4–6), and age was the main predictive variable (odds ratio = 1.5; 95% confidence interval 1.012–2.225; *P* = 0.043). Our series shows cerebrovascular disease incidence of 1.4% in patients with COVID-19 with high morbidity and mortality. We describe pathological and radiological data consistent with thrombotic microangiopathy caused by endotheliopathy with a haemorrhagic predisposition.

Author affiliations

1 Department of Neurology, Hospital General Universitario de Albacete, Albacete, Spain

2 Department of Neurosurgery, Hospital General Universitario de Albacete, Albacete, Spain

3 Department of Surgical Pathology, Hospital General Universitario de Albacete, Albacete, Spain

4 Department of Radiology, Hospital General Universitario de Albacete, Albacete, Spain

5 Anaesthesia Intensive Care Unit, Hospital General Universitario de Albacete, Albacete, Spain

Correspondence to: Francisco Hernández-Fernández

Department of Neurology, Hospital General Universitario de Albacete, Albacete, Spain

E-mail: fco.hdez.fdez@gmail.com

Running title:

Keywords: cerebrovascular disease; COVID-19; endotheliopathy; stroke; SARS-CoV-2

Abbreviations: CVD = cerebrovascular disease; COVID-19 = coronavirus disease 2019; DWI = diffusion weighted imaging; ICA = intracranial carotid artery; mRS = modified

Rankin Scale; SARS-CoV-2 = severe acute respiratory syndrome coronavirus 2; SAH = subarachnoid haemorrhage

Introduction

In December 2019, the first case of severe acute respiratory syndrome coronavirus 2 (SARS-CoV-2) infection was identified in Wuhan, China. Since then, this new coronavirus has spread around the world, causing more than 500 000 deaths to date. On 11 March 2020, the World Health Organization (WHO) declared the situation a pandemic.

The clinical spectrum of coronavirus disease 2019 (COVID-19) ranges from asymptomatic infection to acute respiratory distress syndrome, which requires admission to an intensive care unit. While its main clinical features include fever, cough and dyspnoea, neurological manifestations have also been reported (Helms *et al.*, 2020; Mao *et al.*, 2020).

Several pathophysiological pathways have been proposed that link SARS-CoV-2 infection with a hypercoagulable state, related to cytokine release, microthrombosis and secondary endothelial damage (Ciceri *et al.*, 2020). On the other hand, angiotensin-converting enzyme 2 (ACE2) is the functional receptor of SARS-CoV-2, and is expressed ubiquitously in organs and tissues, constituting a potential target in the endothelium of brain vessels (Varga *et al.*, 2020). ACE2 depletion may have pro-inflammatory and vasoconstrictive effects (Hess *et al.*, 2020).

The estimated incidence of cerebrovascular disease (CVD) among patients infected with SARS-CoV-2 admitted to the hospital is ~2% (Mao *et al.*, 2020). This association appears to worsen the clinical prognosis dramatically, as initial clinical descriptions have shown (Beyrouti *et al.*, 2020; Oxley *et al.*, 2020). Among the common characteristics of these series are a greater tendency to present large vessel occlusion, male predisposition and a more torpid clinical course.

Nevertheless, a better characterization of CVD in SARS-CoV-2 infection is needed. The aim of our study is to describe the clinical characteristics, laboratory findings, neuroimaging and available pathological anatomy data, as well as the presentation, therapeutic management and clinical outcomes of patients with acute CVD in a healthcare setting with a high incidence of transmission of this virus.

Materials and methods

Database and inclusion criteria

The study is a single centre retrospective analysis conducted on a database that included patients in the regional reference unit for the treatment of CVD at the Hospital Universitario de Albacete, Castilla-La Mancha, Spain. We registered all hospitalized patients with COVID-19 reported during this period, and included all patients diagnosed with acute CVD, both ischaemic and haemorrhagic, treated consecutively by neurology, neurosurgery and the intensive care unit.

Patients were included from the date on which the first COVID-19 case was reported in the same health area (1 March 2020) to 19 April 2020. During this period the WHO definition for a confirmed case was: a person with laboratory confirmation of COVID-19 infection, irrespective of clinical signs and symptoms (WHO interim guidance). However, due to the variability in access, analysis and collection of laboratory tests, as well as changing information in regards to sensitivity and specificity data (Fang *et al*., 2020; Li *et al*., 2020*b*), the tests that were considered confirmatory of COVID-19 were the following: (i) positive serological test (IgM/IgG antibodies); (ii) positive PCR (nasopharyngeal exudate); and (iii) typical high resolution chest CT appearance. These cases were subject to notification to of the local health authority and were also treated under the established local protocol of care for patients with COVID-19 (Supplementary Fig. 1).

Analysis of the database was retrospective. All demographic data, times of care, previous comorbidity, clinical scales, treatments, and laboratory data at the time of the stroke were registered in the electronic medical records in a prospective manner. For patients with ischaemic stroke, we recorded stroke aetiology based on the TOAST classification (Adams *et al.*, 1993), and the National Institutes of Health Stroke Scale (NIHSS). Glasgow Coma Scale (GCS) was considered for patients with intracerebral haemorrhage. When epidemiological data and/or symptoms during the previous 15 days were not noted in electronic medical records, the attending doctors communicated directly with patients or their families to ascertain this information.

Clinical-radiological management

The usual working protocols (Hernández-Fernández *et al.*, 2020) were adapted to COVID-19 patient needs, introducing additional microbiological and radiological tests. Patients with ischaemic stroke were initially assessed by a neurologist, basal CT was performed and thrombolytic treatment (alteplase) was administered up to 4.5 h after symptom onset. In cases where mechanical thrombectomy was considered, prior Angio-CT was performed, and in cases of ≥6 h of evolution or undetermined timescale CT perfusion was indicated. Images were analysed by a neuroradiologist, with mechanical thrombectomy considered in patients with large vessel occlusion (M1, M2, ICA, A1, P1, vertebral, basilar). Patients with intracerebral haemorrhage were evaluated by neurology and/or neurosurgery for surgical referral, with Angio-CT or cerebral angiography being considered according to clinical criteria.

All imaging studies were performed with a high resolution 64 multislice Philips Brillance model CT scanner (Koninklijk Philips Electronics). Taking into account the high incidence of COVID-19 transmission in our area during this period, for those patients undergoing studies of other anatomical regions a supplementary chest CT was routinely performed. In addition, all patients admitted to the hospital during this period had a chest X-ray. In cases with pulmonary involvement, typical patterns of COVID-19 were sought (Simpson *et al.*, 2020), and severity was evaluated using the established severity criteria (Li *et al*., 2020). In those patients with an intraparenchymal haemorrhagic component, the volume of the haematoma was calculated using the ABC/2 method (Curtze *et al.*, 2014). The CHARTS classification (Charidimou *et al.*, 2017) was used to categorize intracerebral haemorrhages (superficial, deep and infratentorial, uncertain or multiple). Macrohaemorrhages were identified and defined as ≥4 mm in size (Radmanesh *et al*., 2020). Patients treated by means of revascularization procedures or surgery received another control CT at 24 h to rule out haemorrhagic transformation or re-bleeding. MRIs were performed based on medical judgement, using a Philips Ingenia CX/Achieva dStrem 1.5 T machine.

Endovascular procedures for mechanical thrombectomy were performed on a Philips Azurion 7 B 20/15 biplane angiograph by a single neurointerventionist and an anaesthetist under light sedation. Data on procedure times, number of passes and the thrombolysis in cerebral infarction (TICI) recanalization scale were collected. Surgically treated patients were managed in the intensive care unit. Those patients who did not require invasive treatment were admitted to the stroke unit if they had low suspicion of COVID-19 infection (negative tests and chest CT). The rest were admitted to conventional beds. The clinical prognosis

during hospital admission was determined using the modified Rankin Scale (mRS) scale, a favourable prognosis considered to be mRS ≤ 2, intermediate mRS = 3, and unfavourable mRS 4–6.

The neuropathological study was carried out by an expert neuropathologist, analysing the macro and microscopic characteristics of the brain biopsies and extracted arterial thrombi. Samples were fixed in 4% formaldehyde and embedded in paraffin; 4 µm slices were made and histological samples prepared using haematoxylin and eosin, Gram and Gomori's trichrome stains. Congo red stain was used in cases of intracerebral haemorrhage. For the study of the brain samples, immunohistochemistry techniques were also used: CD34, CD31, ERG (Agilent Technologies) being employed as vascular markers. The morphology and distribution of the red cell series, white cell series, fibrin and the presence or absence of bacteria were also analysed in the arterial thrombi studied.

Statistical analysis

Data were collected and analysed using SPSS version 26 software (SPSS, Chicago, IL, USA). A descriptive study of the variables was performed by calculating central tendency and dispersion measures for the quantitative variables, and the exact calculation and proportion for qualitative variables. Sample normality was determined by means of the Kolmogorov-Smirnov test. Bivariates studies were designed to contrast the main variables among CVD patients, between ischaemic/haemorrhagic subtypes within the COVID-19 group, and to assess clinical prognosis. Proportions were compared using χ^2 square tests or Fisher's exact test, when the sample was too small. The comparison between quantitative variables was conducted by means of the Student *t*-test, or the Mann-Whitney U-test when the data did not follow a normal distribution. For continuous numeric variables, box-and-whisker plots were plotted, indicating mean, median, IQ range, maximum, minimum and outlier values. The independent effect of the variables on prognosis was evaluated with a binary logistic regression model, considering poor prognosis during hospital admission as a dependent variable (mRS 4–6 = bad outcome). Predictors that were found to be related to poor prognosis ($P \leq 0.05$) or with proven prognostic relevance were entered into the model, using stepwise backward selection. Odds ratios (OR) were calculated for each variable. The Cox and Snell R square and Nagelkerke R square values were used to provide information about the amount of variation in the dependent variable. Sensitivity analysis with the Hosmer-

Lemeshow goodness of fit test was conducted to evaluate the overall fit of the data and the influence of the main independent variables. To identify the cut-off point with the best discriminative value of the continuous variable, receiver operating characteristic curve analysis was carried out. A value of $P \leq 0.05$ was considered significant throughout the study.

Ethics

The neurology department has an ongoing inpatient database that includes every single patient with CVD treated in the hospital after having consented. This database is the origin of the present study. This is a retrospective study, the data obtained were not used to modify the usual treatment guidelines. The standards of good clinical practice and the Declaration of Helsinki were followed. The data obtained were kept confidential and used exclusively for study purposes. Informed consent was sought from family members by telephone to authorize use of the data. Written informed consent was waived by the Ethics Commission of the designated hospital under emerging infectious diseases guidelines. The project was presented to the local Clinical Research and Ethics Committee and was approved on 14 April 2020.

Data availability

The authors confirm that the data supporting the findings of this study are available within the article and Supplementary material. Raw data were generated at Hospital Universitario de Albacete. The data that support the findings of this study are available on request from the corresponding author.

Results

A total of 1683 patients with COVID-19 were hospitalized during the 50-day study; of these, 23 patients developed CVD. Most of them (21/23) were confirmed by laboratory criteria, and two by conclusive chest CT findings. Therefore, the incidence of CVD among our patients with COVID-19 infection was 1.4%. During the same period, a total of 89 patients with CVD were admitted to the centre, meaning that 66 cases (74.2%) were most likely stroke patients without COVID-19 infection. With respect to data collected during the same period of time

over the previous 5 years (2014–2019), the mean number of hospital admissions of patients with CVD was slightly higher during the study period (53.4 versus 43.8 cases every month), as well as the mean number of mechanical thrombectomies performed (8.4 versus 5.8 cases every month), whilst the mean number of stroke code activations was the same (33 versus 33 cases every month). Regarding the analysis by aetiology, it should be noted that the number of patients admitted for lacunar stroke was lower (5.3% versus 13%). We have no information about those who were exclusively evaluated in the emergency department, and not considered for further management, so we cannot estimate the prevalence in the general population.

Among patients with CVD and COVID-19, the mean age was 66.8 years, with a male predominance (78.3%). Nineteen of 23 patients (82.6%) had concurrent bilateral interstitial pneumonia at the time of the brain event. In 11 cases (47.8%) no previous respiratory or general symptoms were reported. Among patients with symptoms, the median time from initial COVID-19 symptoms to stroke onset was 5 days. Six patients suffered CVD while in hospital. A summary of the clinical manifestations, treatment administered, analyses and radiological studies of the entire sample is shown in Supplementary Table 1.

Patients with COVID-19 were classified according to the type of CVD: cerebral ischaemia (17/23), intracerebral haemorrhage (5/23), and posterior reversible encephalopathy syndrome (PRES)-type leukoencephalopathy (1/23). Cerebral and chest CT scans were obtained from all patients, and cerebral MRI in only six subjects (26.1%, Patients 7, 19, 21, 13, 15 and 23), due to difficulties in transfer to the MRI room secondary to patient isolation and haemodynamic instability. The overall clinical prognosis of patients with CVD and COVID-19 infection during the hospitalization period was unfavourable in 73.9% (17/23 mRS 4–6). Mortality during this period was high (8/23, 34.8%). The distribution of variables in patients with CVD, and the comparison between the ischaemic and haemorrhagic subtypes are shown in Table 1.

Cerebral ischaemia in COVID-19 patients

A total of 17 patients (73.9%) had COVID-19 and cerebral ischaemia, with a median NIHSS of 16. Ten patients (58.8%) had large vessel occlusion confirmed on non-invasive vascular study (nine with Angio-CT and one with transcranial ultrasound). Three patients did not have a complete vascular study because, after demonstrating extensive cortical infarction on basal CT (presumably large vessel occlusion), no AngioTC was performed for mechanical

thrombectomy planning. Four other cases did not have a proximal occlusion in Angio-CT as previously defined. Based on the TOAST classification, the predominant aetiology was of undetermined origin (52.9%, nine patients), followed by cardioembolism (23.5%, four patients), other determined cause (17.6%, three patients), and intracranial atherothrombotic origin (6%, one patient). No admissions of stroke due to small vessel disease were recorded in the COVID-19 group.

Two of the patients (11.8%, Patients 10 and 16) showed characteristic images of extracranial dissection (Fig. 1). Analysis of the imaging studies identified no cases of cerebral venous thrombosis. Six patients (35.3%, Patients 1, 2, 5, 6, 10 and 15) had vertebrobasilar infarcts, and two patients (Patients 2 and 15) had multi-territory acute infarcts. Patient 15 was initially admitted for a focal deficit condition with epileptic seizures in the form of left hemispheric focal non-convulsive status epilepticus and required sedation and admission to intensive care. After MRI, the presence of acute bihemispheric subcortical ischaemic lesions of the posterior circulation was confirmed (Fig. 2A–C). He was discharged with anti-epileptic drugs and antiplatelet medication but required readmission after 4 weeks due to a transient sensory-motor disorder of the left upper extremity and focal epileptic seizures affecting language. The vascular study was extended to include cerebral angiography, identifying a pattern suggestive of diffuse intracranial arteritis (Fig. 2D–F). Submaximal balloon angioplasty was performed on a significantly stenosed segment of the right intracranial intracranial carotid artery (ICA) bifurcation. High-dose steroids were then administered, successfully eliminating the focal deficit episodes, which allowed brain biopsy to be avoided.

Four patients (23.5%) received intravenous thrombolysis, and five mechanical thrombectomies (29.4%) were performed, two of which were rescue procedures. Endovascular treatments had relatively low technical complexity, with a mean time of 29.4 min, an average of 1.8 passes and a degree of recanalization ≥TICI 2B in all cases (4/5 TICI 2C–3). The remaining patients did not receive revascularization treatment for different reasons (excessive time of evolution, severe haemodynamic instability, extensive established ischaemic injury). The clinical prognosis during the hospitalization period was unfavourable in 11 patients (64.7%), with a mortality of 35.3%.

Intracerebral haemorrhage in COVID-19 patients

Five cases had macrohaemorrhages as previously defined. Four of these patients had SARS-CoV-2 manifestations (80%) at the time of CVD diagnosis. The median time from admission to vascular event was 12 days (IQR 7–16). All patients had previous comorbidities (Supplementary Table 1). The clinical onset was varied, with sudden aphasia, hemiplegia and coma in one patient and seizures in another. The other three haemorrhagic cases were detected on varying days of clinical evolution because having been intubated, sedated and treated for SARS-CoV-2 infection, the neurological manifestations were masked prior to tracheal extubation, when difficulty arousing these patients was observed.

All patients had a brain CT scan, and two brain MRI scans were also performed, one in a postoperative case and the other in an unoperated patient. The severely ill condition of the patients precluded further MRI studies. One preoperative cerebral angiography and one Angio-CT were obtained. Vasculitis, arteriovenous malformations and aneurysms were ruled out.

Patient 18

A 51-year-old female with high blood pressure, smoker, no prior coagulopathy, was admitted to the hospital after a sudden episode of aphasia, right hemiplegia and coma. Brain CT scan showed an extensive left basal ganglia haematoma with ventricular extension. Angio-CT ruled out vascular pathology. Urgent decompressive craniectomy and haematoma evacuation was carried out. No unusual brain tissue findings were reported. The patient died some hours later, with a COVID-19 PCR test proving positive.

Patient 19

A 69-year-old male with known high blood pressure was admitted to the hospital complaining of fever and progressive dyspnoea. As his dyspnoea worsened and a diagnosis of SARS-CoV-2 infection was made, he was transferred to intensive care for mechanical ventilation and further management. Thirteen days later, difficulty arousing him after tracheal extubation prompted a brain CT scan showing a left frontal lobar haematoma (Fig. 4A). The patient underwent left frontal craniotomy for haematoma evacuation. Friable brain tissue with a dark aspect was observed, so a brain biopsy was collected for further study. The main origin of the haematoma was from cortical arterioles. Additional findings were seen in postoperative MRI (Fig. 4B–F).

Patient 20

An otherwise healthy and asymptomatic 61-year-old male was brought to the hospital because of adult onset focal seizures and acute respiratory distress syndrome. A brain CT scan showed a left temporal haematoma with subarachnoid haemorrhage (SAH) extending to the Sylvian fissure (Fig. 5A). Cerebral angiography ruled out vascular pathology. The patient underwent surgical evacuation of the haematoma, intracranial pressure and PtO2 monitoring. Surgical findings were similar to the previous case. A brain biopsy was also collected. PtO2 values were low for the next 3 days. Intracranial pressure was always normal. A PCR test was negative but high resolution chest CT scan, laboratory test findings and clinical course were characteristic of COVID-19, on the basis of a possible false negative the patient was included in this study, but we were unable to conclude investigations. The patient died 10 days later as a result of acute respiratory distress and multiorgan failure.

Patient 21

A 64-year-old male, with high blood pressure, dyslipidaemia, type 2 diabetes mellitus and stable angina was admitted to intensive care because of fever, dyspnoea and severe bilateral interstitial pneumonia. Fifteen days later, a brain CT scan was conducted because of difficulty arousing him after tracheal extubation. CT and MRI findings are described in Fig. 3.

Patient 22

A 68-year-old male, with high blood pressure, dyslipidaemia, type 2 diabetes mellitus and sleep apnoea was admitted to intensive care with fever, dyspnoea and severe bilateral interstitial pneumonia. Sixteen days later, a brain CT scan was conducted because of difficulty arousing him after tracheal extubation. A small left frontal lobar haematoma and SAH were found. CT findings are described in Fig. 5D–F.

Bleeding risk factors

In Patient 18, high blood pressure might play an aetiological role. Patients 19, 21 and 22 were on anticoagulation therapy (enoxaparin 1 mg/kg/twice a day) at the time of bleeding. It should be noted that the CT studies found no chronic lacunar infarcts to support the diagnosis of microangiopathy in any patient. No other potential causes of brain haemorrhage were identified. All patients had poor clinical outcome (mRS 4–6) whilst hospitalized. The mortality rate was 40% in this group.

Leukoencephalopathy

Patient 23 was admitted to the critical care unit for severe pneumonia, and exhibited a low level of consciousness and focal epileptic seizures after extubation. Brain CT scan and Angio-CT were performed showing right occipital hypodensity without vascular stenosis. Cerebral MRI (Fig. 6) demonstrated a PRES-type leukoencephalopathy with micro-bleeding and without diffusion weighted imaging (DWI) alteration. This patient showed several predisposing factors for the development of leukoencephalopathy such as high blood pressure, acute renal failure, sepsis, and had been treated with different immunomodulatory drugs. Once the epileptic seizures were controlled, the neurological course was favourable.

In both of the haemorrhagic patients where MRI was available (Patients 19 and 21) and in the patient with PRES, we observed a similar radiological pattern consisting of bilateral white matter involvement, predominantly parieto-occipital, which spares the periventricular territory and is associated with multiple haemorrhagic lesions, SAH and subcortical microbleeds (Figs 3, 4 and 6).

Neuropathological studies

Neuropathological material was obtained in 6 of 23 cases. Brain biopsy was available from two patients with intracerebral haemorrhage and arterial thrombi from four patients with large vessel occlusion.

Brain biopsies

In both patients there was evidence of a large intraparenchymal haemorrhage; fibrin microthrombi were seen at different points in the brain tissue. The most striking findings were the alterations in the walls of the small arterioles, capillaries and venules, with disappearance of endothelial cells (Fig. 7A–D), degeneration of the neuropil in the periphery of the capillaries due to oedema or extravasation of macromolecules, and local inflammation (Patient 20, Fig. 5B). Fibrinoid necrosis was only found in one small artery. Inflammation of the vascular wall and endothelium was very rare. In viable vessels, the reactive aspect of endothelial cells was striking, and in some cases intranuclear and cytoplasmic clearance were seen (Patient 20, Fig. 5C). Both biopsies were negative for arteriolosclerosis and cerebral amyloid angiopathy was also ruled out.

Extracted arterial thrombi

All were mainly composed of fibrin and red blood cells in variable proportions, but with a predominance of fibrin and different quantities of platelets. In two clots (Patients 3 and 4) apoptotic cells and some endothelial cells (Fig. 7E) were identified within the thrombus along with atypical lymphocytes.

Lung involvement in COVID-19: other associated complications

A total of 19 of 23 patients (82.6%) had simultaneous bilateral interstitial pneumonia at the time of the brain event. Based on the radiological pattern, four cases of mild (17.4%), seven moderate (30.4%), and eight severe (34.8%) pneumonias were identified. Two patients with typical patterns for COVID-19 pneumonia on chest CT and negative microbiological tests are described below.

Patient 1

Ground-glass opacities in lung regions close to visceral pleural surfaces, including the fissures, with a multifocal and bilateral distribution albeit with lower lobe predominance. Pseudonodular consolidations within the ground-glass areas. Subpleural curvilinear bands were noted in the upper lobes.

Patient 20

Initial chest CT showed tenuous ground-glass opacities in lung regions close to visceral pleural surfaces, without consolidation, multifocal and bilateral distribution with upper lobe predominance. A control CT was carried out 10 days later, showing pseudonodular consolidations within the ground-glass areas, with a bilateral multifocal distribution. Extensive lung consolidation and atelectasis of the right lower lobe, with secondary volume loss of the entire hemitorax. Bilateral pleural effusions, greater in the right hemithorax.

Other complications such as bilateral pulmonary embolism in two cases (Patients 9 and 11), ventricular dysfunction (Patients 11 and 12), severe retroperitoneal haematoma (Patient 12) and severe foot ischaemia (Patient 19) were recorded.

Bivariate analysis: sub-analysis of ischaemic and haemorrhagic groups in COVID-19 patients

Bivariate analyses were performed on the main clinical, laboratory tests and radiological characteristics (Table 1). Among the patients who had cerebral ischaemia with COVID-19, higher proportions of large vessel occlusions (58.6 versus 25, $P = 0.031$), median NIHSS (16 versus three, $P = 0.006$), intravenous thrombolysis (20 versus 4.5, $P = 0.043$), mechanical thrombectomy (21.7 versus 13.6, $P = 0.015$), and unfavourable prognosis (73.9 versus 28.8, $P < 0.0001$) were found. In addition, patients with CVD (either ischaemic or haemorrhagic) and COVID-19 had significantly more laboratory test changes (alanine transaminase, C-reactive protein, ferritin), and a lower proportion of previous anticoagulation (42.3 versus 57.7, $P = 0.026$). The proportion of patients with high D-dimer levels was greater in the COVID-19 positive patient group (78.3 versus 19.7, $P = 0.002$). Within the group of patients with COVID-19, bivariate analysis showed that ferritin levels were significantly higher in the haemorrhagic subtype (1554.3 versus 519.2, $P = 0.004$). Box plots of these variables (ferritin and D-dimer) can be seen in Supplementary Fig. 2. The remaining parameters (C-reactive protein, lactate dehydrogenase, haemogram, coagulation) were relatively preserved. The rest of the variables analysed did not show statistical differences. Age was the only variable related to poor clinical prognosis with statistical significance (70.8 versus 55.8, $P = 0.0001$, Supplementary Table 2).

Binary regression logistic and sensitivity analysis

In addition to age, the multivariate model included variables with proven interest that may influence the risk of unfavourable prognosis (sex, intracerebral haemorrhage, large vessel occlusion, severe pulmonary involvement).

Hosmer-Lemeshow's goodness of fit test resulted in χ^2 value = 2.607 (df = 8, $P = 0.957$). The model correctly classified 73.9% of patients with unfavourable clinical prognosis. The significance in the omnibus test in the model was $P = 0.003$. The R-square values of Cox and Snell, and R-square of Nagelkerke were 0.549 and 0.805, respectively.

Binary regression logistic modelling (Supplementary Table 2) showed that age [OR = 1.5; 95% confidence interval (CI) 1.012–2.225; $P = 0.043$], was the only independent predictive factor of unfavourable clinical outcome during admission for CVD with SARS-CoV-2. The

point of maximum diagnostic precision (sensitivity versus specificity) for the incidence of unfavourable prognosis is plotted in a receiver operating characteristic curve (Supplementary Fig. 3), resulting in a cut-off point with a higher area under the curve in patients older than 63 years (AUC 0.907; CI 0.78–1; *P* = 0.003), with sensitivity results of 82.4%, and specificity of 100%.

Discussion

The analysis of our series showed an incidence of CVD of 1.4% in patients admitted with COVID-19 during the study period. The overall clinical outcome of these patients was mostly unfavourable (73.9% mRS 4–6), with a high mortality rate (34.8%). Age was the only independent predictive factor of poor prognosis with a cut-off point set at 63 years old. D-dimer levels were high in most patients, surpassing the threshold identified as a predictor of in-hospital mortality (Zhang *et al.*, 2020). This finding suggests that hypercoagulability could be one of the causes underlying the increased number of cases with undetermined source. A subgroup of critically ill patients with distinctive imaging appearances have been identified showing intracerebral haemorrhage along with leukoencephalopathy but little evidence of sporadic cerebral small vessel disease.

Most cases presented bilateral interstitial pneumonia at the time of the vascular event, with 34.8% of a severe grade. This level of respiratory involvement in patients with CVD is comparable to that reported by a group in Wuhan (Mao *et al.*, 2020). Additionally, high rates of severe systemic complications, such as pulmonary embolism (8.7%) were observed. Patients with cerebral ischaemia and COVID-19 had extensive clinical progression, thrombus load and, consequently, worse clinical prognosis. In line with our results, a recent pooled analysis of 2031 patients of six studies (Aggarwal *et al.*, 2020) showed a 2.5-fold increase in the severity of COVID-19 in CVD patients, as well as a trend towards increased mortality rates.

Within the subgroup of cerebral ischaemia, we encountered a high rate of functional dependence during the hospitalization period (64.7% mRS 4–6), compared to our published registries prior to the pandemic (20–36.5% mRS 4–6). These series include patients without age limit, with any type of ischaemic stroke (Catalá-Ripoll *et al.*, 2020), large vessel occlusion in the anterior circulation (Hernández-Fernández *et al.*, 2020), or in any territory (Hernández-Fernández *et al.*, 2017*b*). Although the follow-up period in these studies was 3

months, it is not sufficient to explain the excess of cases with an mRS 5–6 (41.2%) when associated with COVID-19.

Our mean time from onset of symptoms to neurological assessment has been very long (634 min on average). There are several explanations for this delay: the population may have avoided attending hospitals because of confinement measures, neurological symptoms may have been masked by the infection itself, or a delay in access to neuroimaging or revascularization techniques could be responsible (Oxley *et al.* 2020). We have also detected a reduction in the number of admissions for lacunar-type stroke (5.3% in the global series), which contrasts with previous figures (13%) in our published database (Sánchez-Larsen *et al.*, 2016). In contrast to what has been reported by other groups in Spain (Montaner *et al.*, 2020; Rudilosso *et al.*, 2020; Tejada Meza *et al.*, 2020), the number of admissions, mechanical thrombectomies, and stroke code activations was similar during the study period and our historical cohort. However, it should be noted that our work reflects what happened over a longer period of time and in a more advanced phase of the pandemic than those mentioned above. Although our observed incidence of CVD in COVID-19 patients is slightly lower than reported (Mao *et al.*, 2020), deferred medical care, and the lower number of patients admitted with lacunar infarctions could have underestimated the actual incidence of CVD.

Other reasons that may explain poor prognosis in the group with cerebral ischaemia and COVID-19 could be the high incidence of large vessel occlusion (58.8% had proven occlusions), and vertebrobasilar location (35.3%), which include two patients with acute infarcts in multiple territories. Interestingly, our findings are consistent with the recently described phenotype in a small series, which shows a high incidence of large vessel occlusions, posterior territory predisposition, and multi-territory involvement (Beyrouti *et al.*, 2020). Massive cytokine release and thrombogenesis may contribute to this, as they stimulate the accumulation of coagulation factors in plasma and on the surface of endothelial cells, inducing platelet aggregation in the endothelium. In particular, it is believed that IL-8 and TNFα may stimulate the release of hyperreactive Von Willebrand factor (VWF), and IL-6 inhibits its division (Bernardo *et al.*, 2004). Levels of all these molecules (VWF, IL-6, IL-8 and TNFα) are elevated in patients with SARS-CoV-2 (Henry *et al.*, 2020; Huang *et al.*, 2020), and recently VWF has been identified as a marker of endothelial damage in this disease (Escher *et al.*, 2020). Furthermore, other authors have argued that the mechanisms of

endothelial activation and vascular damage may be the main underpinning of lung damage seen in SARS-CoV-2 (Ciceri *et al.*, 2020).

Additionally, we have seen an unexpected number of arterial dissections (two cases, 11.8%). Although the small sample size (n = 17) prevents us from reaching robust conclusions, the relationship between recent infection, endothelial damage and risk of spontaneous dissection is described (Béjot *et al.*, 2014). In the cases treated by mechanical thrombectomy, we have been able to analyse four extracted arterial thrombi, finding an elevated number of apoptotic cells and activated lymphocytes in two of them. In one of the cases (Fig. 7E) we found detachment of viable endothelial cells towards the lumen of the vessel. We have not previously encountered these findings in our patients, even in samples with marked inflammatory activity and septic embolisms (Hernández-Fernández *et al.*, 2017*b*), which could be a sign of the potential ability of SARS-CoV-2 to promote endothelial damage.

Our study also included patients with CVD caused by haemorrhagic stroke (five cases, 21.7%). SAH and single or multiple intraparenchymal haematomas were constant findings, with an unfavourable prognosis during in-hospital stay. In three of these patients, the vascular event occurred during admission to the intensive care unit, and remained semiologically hidden until extubation. In all of these cases, laboratory parameters compatible with disseminated intravascular coagulation were detected, and they were also under anticoagulant treatment in accordance with local protocols. Intracerebral haemorrhage patients had higher ferritin levels than in the ischaemic group (1554.3 versus 519.2, respectively, P = 0.004), which is one of the cardinal markers of severity in SARS-CoV-2 infection (Henry *et al.*, 2020), suggesting those patients could be in the inflammatory stage of the disease.

Another patient presented with neurological symptoms during the inflammatory phase of SARS-CoV-2 infection, after being extubated. He was classified individually (PRES-type leukoencephalopathy), as despite the fact that the initial neuroimaging mimicked an ischaemic stroke (Fig. 6A), after MRI, signs of posterior PRES-type leukoencephalopathy were confirmed (Fig. 6B and C), with no acute ischaemic lesions in the DWI (Fig. 6D) and little discernible haemorrhagic impact (Fig. 6E). This patient, like most patients in the haemorrhagic subgroup (Figs 3C, 4D and 5E), was intubated, developed characteristic vasogenic white matter oedema and had risk factors (Hefzy *et al.*, 2009; Orhun *et al.*, 2019) that could have contributed to this oedema (sepsis and immunoregulatory drugs, among others). There is no certainty that this leukoencephalopathy is related to the infection, however, we cannot rule out a direct neurotropic effect of SARS-CoV-2, taking into account

that ACE2 is the functional receptor of the virus (Hamming *et al.*, 2004), and which has been previously identified in the endothelial cells of brain arteries and veins (Baig *et al.*, 2020). In fact, selective blocking of ACE2 receptors causes the development of neurogenic hypertension as a result of increased parasympathetic tone and spontaneous baroreflex sensitivity (Fen *et al.*, 2010), a process leading to loss of self-regulation, alteration of the blood–brain barrier, cerebral hypoperfusion and vasogenic oedema (Bartynski, 2008).

This combination of leukoencephalopathy together with intracerebral haemorrhages has been described in some COVID-19 infection series (Kremer *et al*., 2020; Radmanesh *et al*., 2020) and attributed to hypoxia-related changes. However, a similar pattern of leukoencephalopathy and haemorrhages of multiple types and sizes is characteristic of patients with thrombotic microangiopathy caused by severe endothelial injury (Nathanson *et al.*, 2010; Ellchuck *et al.*, 2011). Other authors have studied acute respiratory distress syndrome in critical patients (Radmanesh *et al.*, 2020*b*), with high levels of ferritin, oedema and brain haemorrhages. Although there may be some degree of overlap between our findings and cerebral amyloid angiopathy, our patients did not have other typical features of this pathology, such as increased periventricular signal or occipital cortical microbleeds (Chao *et al*., 2006). Additionally, Congo red stain in the biopsy studies did not show birefringence.

Regarding the neuropathological findings of the biopsies (Figs 5B, C, 7A and D), in both cases there is a marked disappearance of endothelial cells in arterioles, capillaries and venules, together with a low immune response, presumably by activation of apoptosis, as well as nuclear and cytoplasmic clearance that could be related to viral particles, similar to those found in brain endothelial cells in autopsies of patients infected by SARS-CoV-2 (Paniz-Mondolfi *et al.*, 2020). These findings have been described as endotheliitis in a post-mortem analysis of patients infected by SARS-CoV-2 (Varga *et al.*, 2020), and associated with cellular apoptosis via the expression of caspase 3. Conversely, increased endothelial activation at the microcirculation level in response to the release of cytokines and poor cleavage of VWF can induce bleeding (Crawley *et al.*, 2011). In our cases, very few foci of inflammation were found, so we propose that the root cause of the lesion is not an endotheliitis, but an endotheliopathy with extended neuropyl impairment. Notwithstanding, exposure of the basement membrane of brain vessels due to this endotheliopathy may well lead to secondary inflammation albeit of somewhat limited extent.

The findings of the two biopsies and the analysed arterial thrombi could be explained by a cytopathic effect of SARS-CoV-2 on the endothelium, leading to thrombotic

microangiopathy, as there are no histological data in favour of arteriolosclerosis, amyloid angiopathy, vasculitis or necrotizing encephalitis. The lack of scientific knowledge regarding the pathobiology or the neurotropic properties of SARS-CoV-2 means that no particular theory is better than the next. SARS-CoV-2 *in vivo* histological analysis, together with vascular immunohistochemistry markers and Congo red staining can provide valuable information about the endothelium and brain tissue. Furthermore, electron microscopy could help to elucidate the relationship between COVID-19 and endothelial cells with greater clarity.

As to the limitations of our study, first, retrospective analysis may have resulted in several biases. Due to the sample size, the logistic regression was limited to the study of five variables, one of which (age) is continuous. Due to the low number of MRIs performed overall, it is possible that we have omitted relevant data that would help to better characterize the patients (e.g. cerebral venous thrombosis). The classification of Patient 23 on an individual basis (PRES-type leukoencephalopathy) may be somewhat confusing, however, he did not meet clinical-radiological criteria for inclusion in the ischaemic or haemorrhagic groups. Moreover, a patient with high angiographic suspicion of vasculitis ultimately was not subjected to histological study due to his good clinical evolution. The confirmatory microbiological analyses performed on the patients (PCR, serology) were variable. Although the specificity of these tests is high (Li *et al.*, 2020*b*), it is not clear that the reliability is superior to chest CT (Fang *et al.*, 2020; Rubin *et al.*, 2020), therefore, considering the epidemiological context, in cases of high radiological suspicion, we continued the investigation as with any other SARS-CoV-2 infection, and the same therapeutic protocol was applied. In two cases the diagnosis was based on chest CT, as the investigation could not be completed due to death (Patient 20) and early discharge from hospital (Patient 1).

In conclusion, our pathological samples, which show the aforementioned characteristics, suggest that endothelial disruption is the primary mechanism of damage. Furthermore, neuroimaging tests indicate that thrombotic microangiopathy, loss of self-regulation and increased bleeding predisposition also co-exist in patients with SARS-CoV-2. In addition, increased hypercoagulability and systemic complications leads to a deterioration in the clinical prognosis of these patients.

Acknowledgements

Thanks to Dr Raquel López, Dr Marisa Tercero for their special dedication, and Dr Javaad Ahmad for the revision of the English translation. We acknowledge the work of the other members of the Neurology, Neurosurgery, Radiology and Anaesthesiology Services for the clinical management of these patients, in addition to the collaboration of the Internal Medicine, Microbiology, Clinical Analysis, Emergency and Intensive Care Services in the preparation of protocols and medical care. We are grateful for the commendable efforts of the nursing staff and other health professionals during the most serious phases of the pandemic, as well as the strength and fortitude which family members and patients have displayed in the face of immense suffering.

Funding

No funding has been required in connection with the preparation of this manuscript.

Competing interests

The authors report no competing interests.

Supplementary material

Supplementary material is available at *Brain* online.

References

Adams HP Jr, Bendixen BH, Kappelle LJ, Biller J, Love BB, Gordon DL, et al. Classification of subtype of acute ischemic stroke. Definitions for use in a multicenter clinical trial. TOAST. Trial of Org 10172 in Acute Stroke Treatment. Stroke 1993; 24: 35-41.

Aggarwal, G, Lippi, G, Michael Henry, B. Cerebrovascular disease is associated with an increased disease severity in patients with Coronavirus Disease 2019 (COVID-19): A pooled analysis of published literature. International Journal of Stroke 2020 10.1177/1747493020921664.

Baig AM, Khaleeq A, Ali U, Syeda H. Evidence of the COVID-19 Virus Targeting the CNS: Tissue Distribution, Host-Virus Interaction, and Proposed Neurotropic Mechanisms. ACS Chem Neurosci 2020; 11: 995-998.

Bartynski WS. Posterior reversible encephalopathy syndrome, part 2: controversies surrounding pathophysiology of vasogenic edema. [Review]. AJNR Am J Neuroradiol 2008; 29: 1043-9.

Béjot Y, Aboa-Eboulé C, Debette S, Pezzini A, Tatlisumak T, Engelter S, et al. Characteristics and outcomes of patients with multiple cervical artery dissection. Stroke 2014; 45: 37-41.

Bernardo A, Ball C, Nolasco L, Moake JF, Dong JF. Effects of inflammatory cytokines on the release and cleavage of the endothelial cell-derived ultralarge von Willebrand factor multimers under flow. Blood 2004; 104: 100-6.

Beyrouti R, Adams ME, Benjamin L, Cohen H, Farmer SF, Goh YY, et al. Characteristics of ischaemic stroke associated with COVID-19. J Neurol Neurosurg Psychiatry 2020 10.1136/jnnp-2020-323586

Catalá-Ripoll JV, Monsalve-Naharro JÁ, Hernández-Fernández F. Incidence and predictive factors of diaphragmatic dysfunction in acute stroke. BMC Neurol 2020; 20: 79.

Chao CP, Kotsenas AL, Broderick DF. Cerebral Amyloid Angiopathy: CT and MR Imaging Findings. [Review]. Radiographics 2006; 26: 1517-1531.

Charidimou A, Schmitt A, Wilson D, Yakushiji Y, Gregoire SM, Fox Z, et al. The Cerebral Haemorrhage Anatomical RaTing inStrument (CHARTS): Development and assessment of reliability. J Neurol Sci 2017; 372: 178-183.

Curtze S, Strbian D, Meretoja A, Putaala J, Eriksson H, Haapaniemi E, et al. Higher baseline international normalized ratio value correlates with higher mortality in intracerebral hemorrhage during warfarin use. Eur J Neurol 2014; 21: 616-22.

Ciceri F, Beretta L, Scandroglio AM, Colombo S, Landoni G, Ruggeri A, et al. Microvascular COVID-19 lung vessels obstructive thromboinflammatory syndrome (MicroCLOTS): an atypical acute respiratory distress syndrome working hypothesis. Crit Care Resusc 2020 Pubmed PMID: 32294809

Crawley JT, de Groot R, Xiang Y, Luken BM, Lane DA. Unraveling the scissile bond: how ADAMS13 recognizes and cleaves von Willebrand factor. Blood 2011; 118: 3212-3221.

Ellchuk TN, Shah LM, Hewlett RH, Osborn AG. Suspicious neuroimaging pattern of thrombotic microangiopathy. AJNR Am J Neuroradiol 2011; 32: 734-8.

Escher R, Breakey N, Lämmle B. Severe COVID-19 infection associated with endothelial activation. Thromb Res 2020 10.1016/j.thromres.2020.04.014

Fang Y, Zhang H, Xie J, Lin M, Ying L, Pang P, et al. Sensitivity of Chest CT for COVID-19: Comparison to RT-PCR. Radiology 2020 10.1148/radiol.2020200432

Fen Y, Xia H, Cai Y, Halami CM, Becker LK, Santos RAS, et al. Brain-selective over-expression of human Angiotensin Converting Enzyme 2 attenuates neurogenic hypertension. Circ Res 2010; 106: 373.

Hamming I, Timens W, Bulthuis ML, Lely AT, Navis G, van Goor H. Tissue distribution of ACE2 protein, the functional receptor for SARS coronavirus. A first step in understanding SARS pathogenesis. J Pathol 2004; 203: 631-7.

Hefzy HM, Bartynski WS, Boardman JF, Lacomis D. Hemorrhage in posterior reversible encephalopathy syndrome: imaging and clinical features. AJNR Am J Neuroradiol 2009; 30: 1371-9.

Henry BM, de Oliveira MHS, Benoit S, Plebani M, Lippi G. Hematologic, biochemical and immune biomarker abnormalities associated with severe illness and mortality in coronavirus disease 2019 (COVID-19): a meta-analysis. Clin Chem Lab Med 2020 10.1515/cclm-2020-0369

Helms J, Kremer S, Merdji H, Clere-Jehl R, Schenck M, Kummerlen C, et al. Neurologic Features in Severe SARS-CoV-2 Infection. N Engl J Med 2020 10.1056/NEJMc2008597

Hernández-Fernández F, Del Valle Pérez JA, García-García J, Ayo-Martín Ó, Ramos-Araque ME, Molina-Nuevo JD, et al. Simultaneous Angioplasty and Mechanical Thrombectomy in Tandem Carotid Occlusions. Incidence of Reocclusions and Prognostic Predictors. J Stroke Cerebrovasc Dis 2020; 29: 104578.

Hernández-Fernández F, Rojas-Bartolomé L, García-García J, Ayo-Martín Ó, Molina-Nuevo JD, Barbella-Aponte RA, et al. Histopathological and Bacteriological Analysis of Thrombus Material Extracted During Mechanical Thrombectomy in Acute Stroke Patients. Cardiovasc Intervent Radiol 2017b; 40: 1851-1860.

Hess DC, Eldahshan W, Rutkowski E. COVID-19-Related Stroke. Transl Stroke Res 2020; 11: 322-325.

Huang C, Wang Y, Li X, Ren L, Zhao J, Hu Y, et al. Clinical features of patients infected with 2019 novel coronavirus in Wuhan, China. Lancet 2020; 395: 497-506.

Kremer S, Lersy F, de Sèze J, Ferré JC, Maamar A, Carsin-Nicol B, et al. Brain MRI Findings in Severe COVID-19: A Retrospective Observational Study. Radiology 2020 10.1148/radiol.2020202222

Li K, Fang Y, Li W, Pan C, Qin P, Zhong Y, et al. CT image visual quantitative evaluation and clinical classification of coronavirus disease (COVID-19). Eur Radiol 2020 10.1007/s00330-020-06817-6

Li Z, Yi Y, Luo X, Xiong N, Liu Y, Li S, et al. Development and clinical application of a rapid IgM-IgG combined antibody test for SARS-CoV-2 infection diagnosis. J Med Virol 2020b 10.1002/jmv.25727

Mao L, Jin H, Wang M, Hu Y, Chen S, He Q, et al. Neurologic Manifestations of Hospitalized Patients With Coronavirus Disease 2019 in Wuhan, China. JAMA Neurol 2020 10.1001/jamaneurol.2020.1127

Montaner J, Barragán-Prieto A, Pérez-Sánchez S, Escudero-Martínez I, Moniche F, Sánchez-Miura JA, et al. Break in the Stroke Chain of Survival Due to COVID-19. Stroke 2020 10.1161/STROKEAHA.120.030106

Nathanson S, Kwon T, Elmaleh M, Charbit M, Launay EA, Harambat J, et al. Acute neurological involvement in diarrhea-associated hemolytic uremic syndrome. Clin J Am Soc Nephrol 2010; 5: 1218-28.

Orhun G, Esen F, Özcan PE, Sencer S, Bilgiç B, Ulusoy C, et al. Neuroimaging Findings in Sepsis-Induced Brain Dysfunction: Association with Clinical and Laboratory Findings. Neurocrit Care 2019; 30: 106-117.

Oxley TJ, Mocco J, Majidi S, Kellner CP, Shoirah H, Singh IP, et al. Large-Vessel Stroke as a Presenting Feature of Covid-19 in the Young. N Engl J Med 2020 10.1056/NEJMc2009787

Paniz-Mondolfi A, Bryce C, Grimes Z, Gordon RE, Reidy J, Lednicky J, et al. Central Nervous System Involvement by Severe Acute Respiratory Syndrome Coronavirus -2 (SARS-CoV-2). J Med Virol 2020 10.1002/jmv.25915

Radmanesh A, Derman A, Lui YW, Raz E, Loh JP, Hagiwara M, et al. COVID-19 - Associated Diffuse Leukoencephalopathy and Microhemorrhages. Radiology 2020 10.1148/radiol.2020202040.

Radmanesh F, Rodriguez-Pla A, Pincus MD, Burns JD. Severe cerebral involvement in adult-onset hemophagocytic lymphohistiocytosis. J Clin Neurosci 2020b 10.1016/j.jocn.2020.04.054

Rubin GD, Ryerson CJ, Haramati LB, Sverzellati N, Kanne JP, Raoof S, et al. The Role of Chest Imaging in Patient Management during the COVID-19 Pandemic: A Multinational Consensus Statement from the Fleischner Society. Chest 2020 10.1016/j.chest.2020.04.003

Rudilosso S, Laredo C, Vera V, Vargas M, Renu A, Llull L, et al. Acute Stroke Care Is at Risk in the Era of COVID-19: Experience at a Comprehensive Stroke Center in Barcelona. Stroke 2020; 51: 1991-1995.

Sánchez-Larsen Á, García-García J, Ayo-Martín O, Hernández-Fernández F, Díaz-Maroto I, Fernández-Díaz E, et al. Has the aetiology of ischaemic stroke changed in the past decades? Analysis and comparison of data from current and historical stroke databases. Neurologia 2016 10.1016/j.nrl.2016.07.003

Simpson S, Kay FU, Abbara S, Bhalla S, Chung JH, Chung M, et al. Radiological Society of North America Expert Consensus Statement on Reporting Chest CT Findings Related to COVID-19. Endorsed by the Society of Thoracic Radiology, the American College of Radiology, and RSNA. J Thorac Imaging 2020 10.1097/RTI.0000000000000524

Tejada Meza H, Lambea A, Sancho Saldaña A, Martínez-Zabaleta mechanical thrombectomy, de la Riva P, López-Cancio E, et al. Impact of COVID-19 Outbreak in Ischemic Stroke Admissions and In-Hospital Mortality in North-West Spain. Int J Stroke 2020 10.1177/1747493020938301

Varga Z, Flammer AJ, Steiger P, Haberecker M, Andermatt R, Zinkernagel AS, et al. Endothelial cell infection and endotheliitis in COVID-19. Lancet 2020 10.1016/S0140-6736(20)30937-5

World Health Organization. Clinical management of severe acute respiratory infection (SARI) when COVID-19 disease is suspected. https://www.who.int/publications-detail/clinical-management-of-severe-acute-respiratory-infection-when-novel-coronavirus-(ncov)-infection-is-suspected. Published March 13,2020.

Zhang L, Yan X, Fan Q, Liu H, Liu X, Liu Z, et al. D-dimer levels on admission to predict in-hospital mortality in patients with Covid-19. J Thromb Haemost 2020 10.1111/jth.14859

Figure legends

Figure 1 Arterial dissections. (**A**–**C**) Patient 10. (**A**) Angio-CT of supra-aortic trunk curved reconstruction along the left vertebral artery path, where the presence of an intimal flap (*arrow*) is proven, showing the existence of a dissection, as well as pseudo-occlusion of the proximal portion. (**B**) Selective angiography of right vertebral artery, in lateral projection, showing complete occlusion of the distal basilar artery. (**C**) Right vertebral artery angiography, anterioposterior (AP) projection, showing basilar recanalization after aspiration mechanical thrombectomy. (**D**–**F**) Patient 16. (**D**) Angio-CT of supra-aortic trunk, sagittal reconstruction, showing dissection at the origin of the right ICA, with an evident intimal flap. (**E**) Angio-CT of the circle of Willis, oblique coronal reconstruction, showing occlusion of an insular branch of the upper division of the right middle cerebral artery (*arrow*). (**F**) The existence of subacute ischaemic lesions in the right middle cerebral artery (insular and temporo-occipital transition) can be seen.

Figure 2 Patient 15. (**A**) MRI, T_2*-weighted fast gradient echo sequence observing multiple microbleeding foci. (**B**) Diffusion alteration focus in relation to acute ischaemic injury. (**C**) Fluid-attenuated inversion recovery (FLAIR) sequence showing signal alteration of the deep white matter, both supra and infratentorial, with involvement mainly of basal ganglia,

thalamus, brainstem and cerebellar hemispheres. (**D**) Right vertebral artery selective angiography, lateral projection, in which multiple focal stenoses in V4 segment and wall irregularity of several small calibre arterial branches are observed. (**E**) Angiography of right ICA, AP projection, showing critical stenosis of right ICA bifurcation. (**F**) Angiography of right ICA, AP projection. Arteriographic control showing partial recovery of vascular calibre after submaximal angioplasty using a Gateway catheter-balloon (Boston Scientific Co) of 2.5 mm × 15 mm. The findings of these studies are suggestive of CNS vasculitis, although no biopsy was obtained.

Figure 3 Patient 21. (**A**) Basal CT. Focal cortico-subcortical haemorrhages (*arrowhead*), and multiple foci of associated SAH (*red arrow*). (**B**–**D**) FLAIR MRI. Affectation of the cortico-subcortical white matter, parieto-occipital and bilateral cerebellar (*asterisk*) and SAH (*red arrow*) is observed. (**E**) DWI. No alteration is observed. (**F**) T_2*-weighted fast gradient echo MRI. Multiple images of cortico-subcortical haemorrhages that appear hypointense (*arrowheads*) and are heterogeneous in DWI sequence (**E**) and hyperintense with a hypointense ring in FLAIR sequence (**B**).

Figure 4 Patient 19. (**A**) Basal CT. Bilateral parieto-occipital white matter involvement with extension to semi-oval centres, left frontal intraparenchymal haematoma (*arrowhead*) and right frontal SAH (*red arrow*). (**A** and **C**) Post-surgical MRI. T_2*-weighted fast gradient echo. Left frontal post-surgical changes. Multiple very hypointense foci due to left frontal bleeding (*arrowhead*) as well as multiple cortico-subcortical microhaemorrhages (*yellow arrows*). (**D and E**) FLAIR MRI. Hyperintensity of the bilateral parieto-occipital white matter in border territories with extension to semi-oval centres (*blue star*). (**F**) DWI. The lesions described in **D** and **E** are not associated with alteration in the DWI sequence.

Figure 5 Patient 20. (**A**) Basal CT. Left intraparenchymal temporal haematoma (*arrowhead*) with associated SAH (*red arrow*). (**B**) Brain biopsy. Haematoxylin and eosin ×20 staining. Area with disappearance of endothelial cells (*ellipse*), area of vascular wall preserved (*box*), reactive endothelial cells with hyperchromatic nuclei (*arrowhead*). In the periphery of the vessel, neuropil degeneration is observed (*small arrows*). (**C**) The *upper* image shows nuclear clearance of the cells and incipient neuronal damage. In the *lower* image, parenchyma with

significant oedema, evident neuronal damage and a vessel with light occluded by endothelial reactivity. (**D**–**F**) Patient 22. Basal CT. Left frontal millimetre haemorrhage (*arrowhead*), small right frontal SAH (*red arrow*) and slight hypodensity in right parieto-occipital white matter (*blue star*).

Figure 6. Patient 23 (**A**) Basal CT. Right parieto-occipital hypodensity (*asterisk*). (**B** and **C**) MRI. FLAIR sequence showing hyperintensity of the bilateral parieto-occipital white substance in border territory with patchy extension to the left semi-oval centre and a right frontal cortical hyperintensity (*arrowhead*). (**D**) DWI. No alteration is seen. (**E**) T_2*-weighted fast gradient echo MRI. Multiple hypointensities indicative of cortical-subcortical micro-bleeding (*yellow arrow*). (**F**) Chest X-ray where the presence of a diffuse interstitial pattern associating consolidations in both lung bases is observed. A pattern suggestive of COVID-19 infection.

Figure 7 Patients 19 and 3. (**A**–**D**) Patient 19 brain biopsy. Haematoxylin and eosin ×20 staining. (**A**) Three microthrombi are observed (*arrowhead*). (**B**) Image with three vessels (*arrows*): the *upper* one preserved with endothelial reactivity, *intermediate* vessel with preserved structure without viable cellularity. The *lower* one shows loss of endothelial cells. (**C**) Capillary with evident alteration of endothelial cells and loss of adhesion (*thin arrow*). Extravasation of inflammatory cells with atypical lymphocytes in the perivascular space. (**D**) Image of arteries and arterioles with reactive endothelial cells (*arrowhead*), some in the vessel lumen (*small arrow*) and normal endothelium (*large arrow*). (**E**) Patient 3. Thrombotic material from a mechanical thrombectomy. Some endothelial cells (*blue star*) are observed.

	COVID-19+ *n* = 23	**COVID-19− *n* = 66**	***P***	**COVID-19+ and cerebral ischaemia *n* = 17**	**COVID-19+ and ICH *n* = 5**	***P***
Age	66.9 ± 11.8	68 ± 14.7	0.75	68.2 ± 13	62.6 ± 7.2	0.24
Sex, male	18 (78.3)	48 (72.7)	0.6	13 (76.5)	4 (80)	1
High blood pressure	15 (65.2)	39 (59.1)	0.6	10 (58.8)	4 (80)	0.61
Type 2 diabetes mellitus	9 (39.1)	21(31.8)	0.53	6 (35.3)	2 (40)	1
Dyslipidaemia	10 (43.5)	28 (42.4)	0.93	7 (41.3)	3 (60)	0.62
Current smoking	3 (13)	14 (21.2)	0.64	2 (11.8)	1 (20)	1
Ischaemic heart disease	4 (17.4)	10 (15.2)	0.8	4 (23.5)	0 (0)	0.22
Atrial fibrillation	4 (21.4)	18 (30.5)	0.42	4 (23.5)	0 (0)	0.53
COPD	2 (8.7)	4 (6.1)	0.52	2 (11.8)	0 (0)	0.6
Baseline NIHSS[a], median [IQR]	16 [9–24]	3 [0–8]	**0.006**	16 [9–24]	N/A	N/A
Baseline GCS[b], median [range]	8 [3–11]	6 [3–15]	0.8	N/A	8 [3–11]	N/A
Time to onset – neurological assessment[a], min	634.3 ± 839.6	987.4 ± 2245	0.41	634.3 ± 839.6	N/A	N/A
Parenchymal haemorrhage volume[b], cm^3 mean [range]	41.9 [0.4–125]	53.7 [1.6–149.2]	0.71	N/A	41.9 [0.4–125]	N/A
Haemoventricle[b]	1 (20)	7 (50)	0.6	N/A	1 (20)	N/A
CHARTS[b]			0.4	N/A		N/A
Superficial	3 (60)	5 (35.7)			3 (60)	
Deep and infrantentorial	1 (20)	5 (35.7)			1 (20)	
Uncertain and multiple	1 (20)	2 (14.3)			1 (20)	
Pure intraventricular or SAH	0 (0)	2 (14.3)				
Previous respiratory or other general symptoms	12 (52.2)	N/A	N/A	6 (35.3)	4 (80)	0.13
Moderate-severe pneumonia caused by COVID-19	15 (65.2)	N/A	N/A	10 (58.8)	4 (80)	0.61
Prior anticoagulation	11 (42.3)	15 (57.7)	**0.026**	7 (41.2)	3 (60)	0.62
Ferritin, ng/ml	717.3 ± 645.8	239.7 ± 289.1	**0.005**	519.2 ± 473.7	1554.3 ± 815.4	**0.004**
Alanine transaminase, U/l	38.6 ± 33	24.2 ± 26.5	**0.041**	53.3 ± 99.2	78 ± 49	0.6
C-reactive protein, mg/dl	28.8 ± 37.1	10.3 ± 21.8	**0.048**	36.3 ± 39.6	11 ± 16.9	0.24
Lactate dehydrogenase, U/l	270.7 ± 113.1	221.5 ± 135.2	0.1	257.2 ± 119.5	342 ± 69.8	0.15
Platelets, $x10^3$/mcl	242.5 ± 122.9	216.7 ± 88.3	0.28	266.8 ± 120.6	211 ± 127.7	0.38
Lymphocytes, /mcl	1243 ± 741.8	1777.3 ± 1271.4	0.06	1364 ± 672.6	1108 ± 1082	0.52
Fibrinogen, mg/dl	360.6 ± 89.5	319.7 ± 81.8	0.06	344.5 ± 271.5	355.6 ± 88.6	0.81
D-dimer, µg/l	7148.1 ± 16 369	2908.1 ± 12 507	0.34	8644.7 ± 23 256.1	3387.8 ± 1116.5	0.63
D-dimer, >500 µg/l	18 (78.3)	13 (19.7)	**0.002**	12 (70.6)	5 (100)	0.54
Partial thromboplastin time, s	29.1 ± 5.4	30.7 ± 5	0.22	29.5 ± 6	27 ± 2.7	0.4
Lacunar stroke[a]	0 (0)	4 (6.1)	0.12	0 (0)	N/A	N/A
Large vessel occlusion[a]	10 (58.8)	13 (25)	**0.031**	10 (58.8)	N/A	N/A
Intravenous alteplase[a]	4 (20)	3 (4.5)	**0.043**	4 (23.5)	N/A	N/A
Mechanical thrombectomy[a]	5 (21.7)	9 (13.6)	**0.015**	5 (29.4)	N/A	N/A
Time of the procedure[a], min	29.4 ± 12.2	36.6 ± 16.8	0.7	29.4 ± 12.2	N/A	N/A
Number of passes[a]	1.8 ± 0.83	2.5 ± 1.1	0.3	1.8 ± 0.83	N/A	N/A
Haemorrhagic transformation/rebleeding	0 (0)	0 (0)	1	0 (0)	0 (0)	1
mRS 4–6	17 (73.9)	19 (28.8)	**<0.0001**	11 (64.7)	5 (100)	0.27
Mortality	7 (30.4)	9 (13.6)	0.08	5 (29.4)	2 (40)	0.66

Table 1 Description and frequency of baseline characteristics, comorbidity, clinical, laboratory, radiological and prognostic variables in patients with CVD

Values are presented as *n* (%) or mean ± SD unless otherwise stated. Comparison between patients with and without SARS-CoV-2 infection, and subanalysis among the groups with SARS-CoV-2 (cerebral ischaemia and ICH). Statistically significant results are highlighted in bold. COPD = chronic obstructive pulmonary disease; GCS = Glasgow Coma Scale; ICH = intracerebral haemorrhage; N/A = not aplicable; NIHSS = National Institutes of Health Stroke Scale.

[a]Calculated over the patients with cerebral ischaemia; [b]calculated over the patients with ICH.

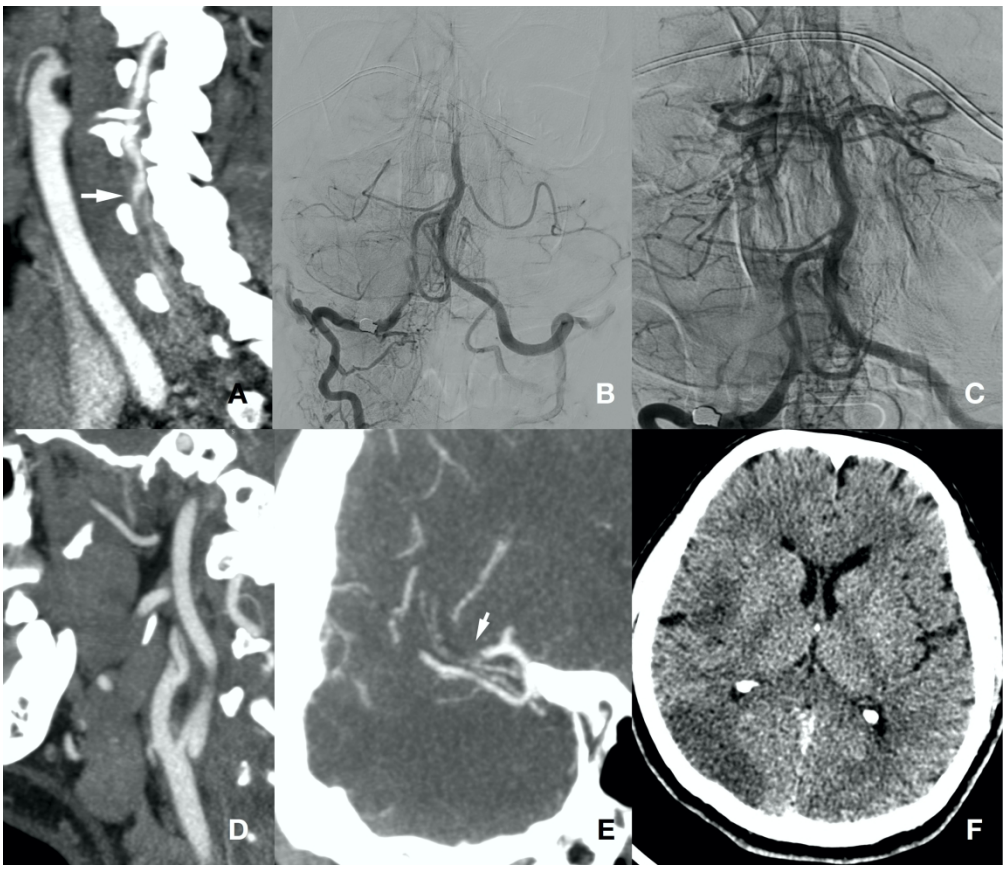

Figure 1. Arterial dissections. Patient 10 (A-C). A: AngioCT of SAT curved reconstruction along the left VA path, where the presence of an intimal flap (arrow) is proven, showing the existence of a dissection, as well as pseudo-occlusion of the proximal portion. B: Selective angiography of right VA, in lateral projection, showing the presence of floating thrombus in the basilar artery. C: Right VA angiography, AP projection, showing basilar recanalization after aspiration MT. Patient 16 (D-F). D: AngioCT of SAT, sagittal reconstruction, showing dissection at the originof the right ICA, with an evident intimal flap. E: AngioCT of the Circle of Willis, oblique coronal reconstruction, showing occlusion of an insular branch of the upper division of the right MCA (arrow). F: The existence of subacute ischaemic lesions in the right MCA (insular and temporo-occipital transition) can be seen.

279x240mm (300 x 300 DPI)

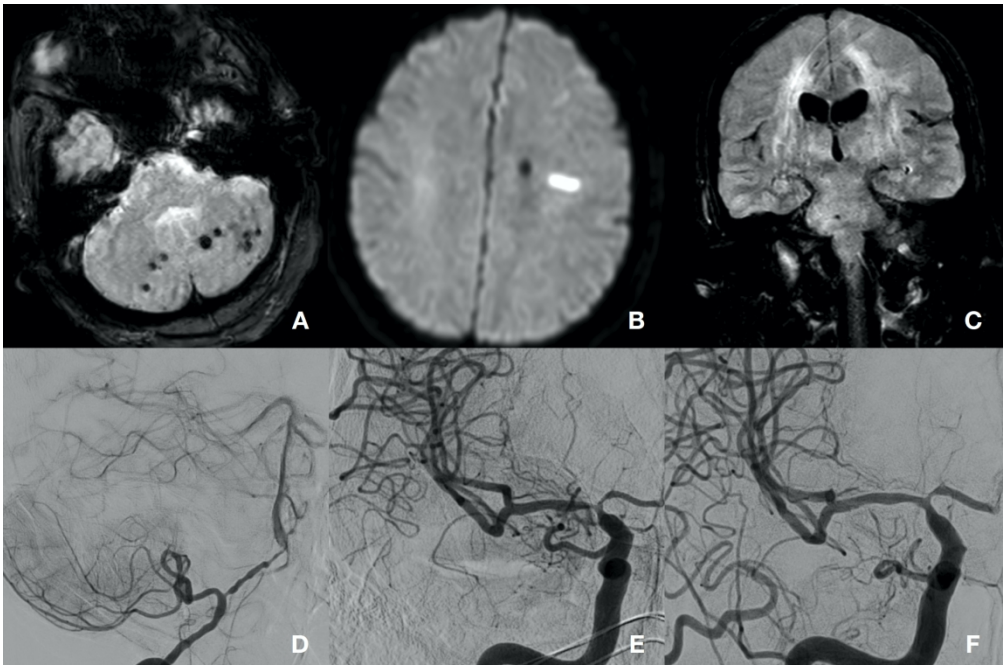

Figure 2. Patient 15 (A-F). A: MRI, FFE*T2 sequence observing multiple microbleeding foci. B: Diffusion alteration focus in relation to acute ischaemic injury. C: FLAIR sequence showing signal alteration of the deep white matter, both supra and infratentorial, with involvement mainly of basal ganglia, thalamus, brain stem and cerebellar hemispheres. D: Right VA selective angiography, lateral projection, in which multiple focal stenoses in V4 segment and wall irregularity of several small calibre arterial branches are observed. E: Angiography of right ICA, AP projection, showing critical stenosis of right ICA bifurcation. F: Angiography of right ICA, AP projection. Arteriographic control showing partial recovery of vascular calibre after submaximal angioplasty using a Gateway catheter-balloon (Boston Scientific Co, Fremont, CA, USA) of 2.5 mm x 15 mm. The findings of these studies are suggestive of central nervous system vasculitis, although no biopsy was obtained.

214x141mm (300 x 300 DPI)

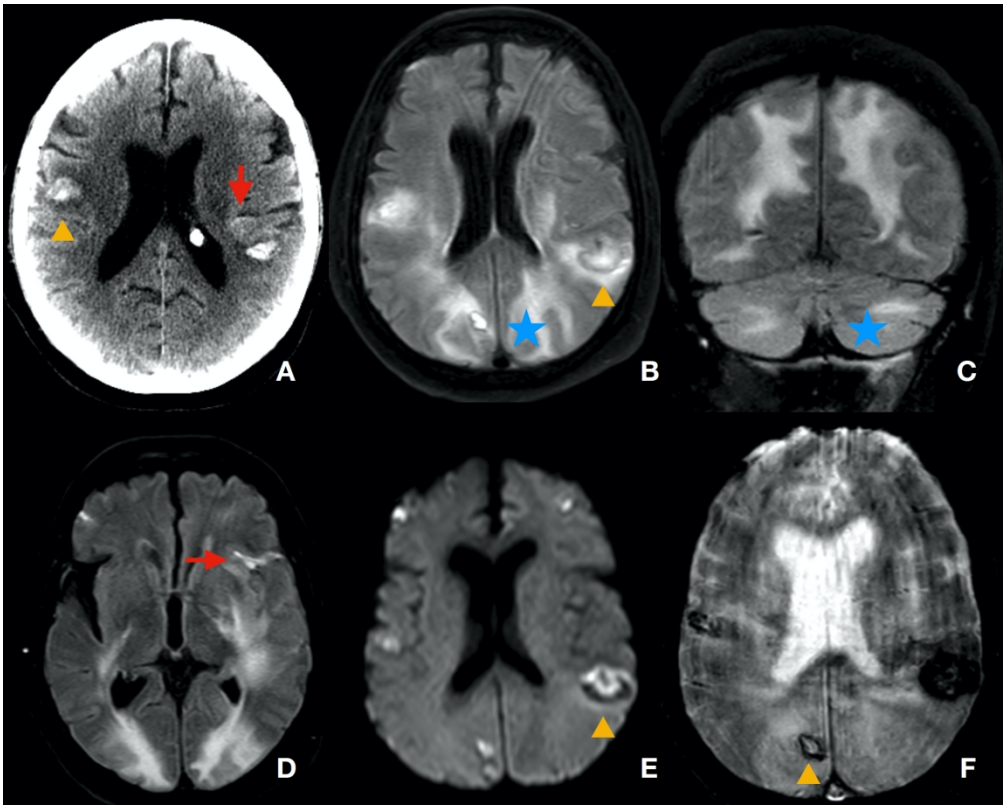

Figure 3. Patient 21 (A-F). A: Basal CT. Focal cortico-subcortical haemorrhages (arrowhead), and multiple foci of associated SAH (red arrow). B, C and D: MRI. FLAIR. Affectation of the cortico-subcortical white matter, parieto-occipital and bilateral cerebellar (asterisk) and SAH (red arrow) is observed. E: DWI. No alteration is observed. F: FFE*T2. Multiple images of cortico-subcortical haemorrhages that appear hypointense (arrowheads) and are heterogeneous in DWI sequence (E) and hyperintense with a hypointense ring in FLAIR sequence (B).

189x151mm (300 x 300 DPI)

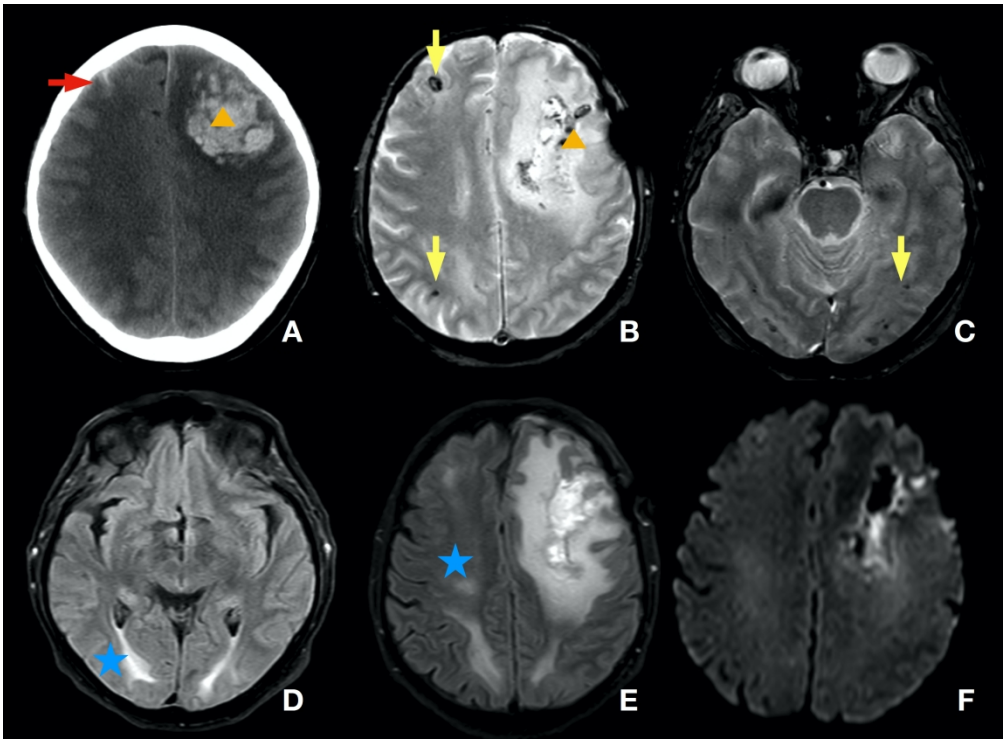

Figure 4. Patient 19 (A-F). A: Basal CT. Bilateral parieto-occipital white matter involvement with extension to semioval centres, left frontal intraparenchymal haematoma (arrowhead) and right frontal SAH (red arrow). B and C: Post-surgical MRI. FFE* T2. Left frontal post-surgical changes. Multiple very hypointense foci due to left frontal bleeding (arrowhead) as well as multiple cortico-subcortical microhaemorrhages (yellow arrows). D and E: FLAIR. Hyperintensity of the bilateral parieto-occipital white matter in border territories with extension to semioval centers (blue star). F: DWI. The lesions described in D and E are not associated with alteration in the DWI sequence.

557x410mm (144 x 144 DPI)

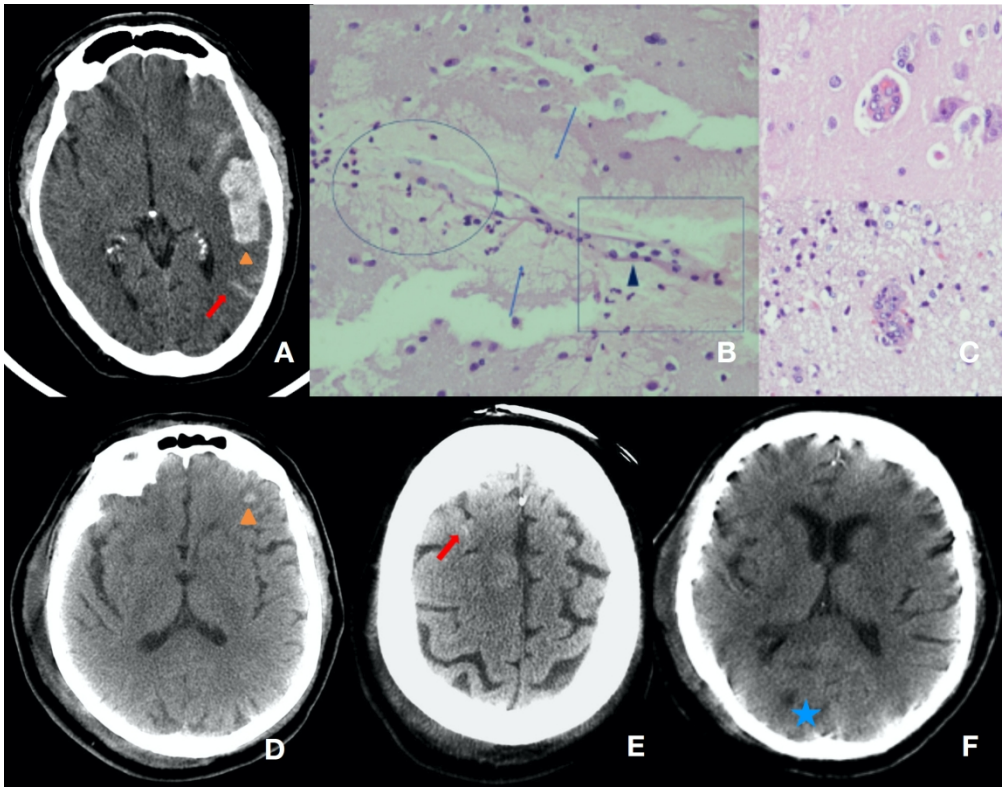

Figure 5. Patient 20 (A-C). A: Basal CT. Left intraparenchymal temporal haematoma (arrowhead) with associated SAH (red arrow). B: Brain biopsy. HEx20 staining. Area with disappearance of endothelial cells (ellipse), area of vascular wall preserved (box), reactive endothelial cells with hyperchromatic nuclei (arrowhead). In the periphery of the vessel, neuropil degeneration is observed (small arrows). C: The upper image shows nuclear clearance of the cells and incipient neuronal damage. In the lower image, parenchyma with significant oedema, evident neuronal damage and a vessel with light occluded by endothelial reactivity. Patient 22 (D-F). D, E, F: Basal CT. Left frontal millimetre haemorrhage (arrowhead), small right frontal SAH (red arrow) and slight hypodensity in right parieto-occipital white matter (blue star).

181x141mm (300 x 300 DPI)

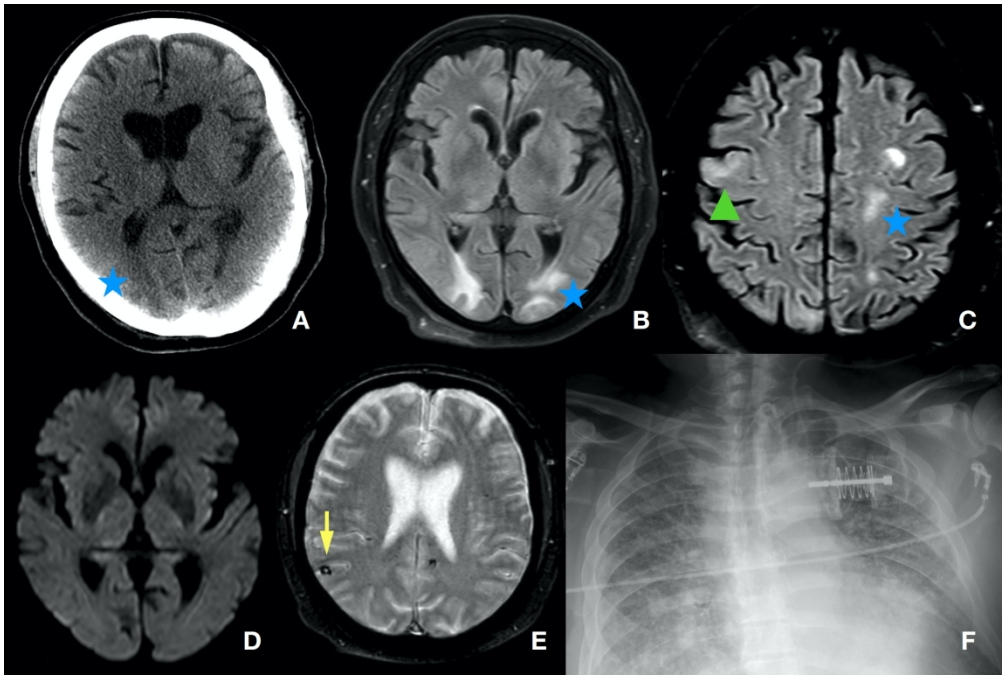

Figure 6. Patient 23 (A-F). A: Basal CT. Right parieto-occipital hypodensity (asterisk). B and C: MRI. FLAIR sequence showing hyperintensity of the bilateral parieto-occipital white substance in border territory with patchy extension to the left semioval center and a right frontal cortical hyperintensity (arrowhead). D: DWI. No alteration is seen. E: FFE*T2. Multiple hypointensities indicative of cortical-subcortical micro-bleeding (yellow arrow). F: X-Ray Chest where the presence of a diffuse interstitial pattern associating consolidations in both lung bases is observed. A pattern suggestive of COVID-19 infection.

207x138mm (300 x 300 DPI)

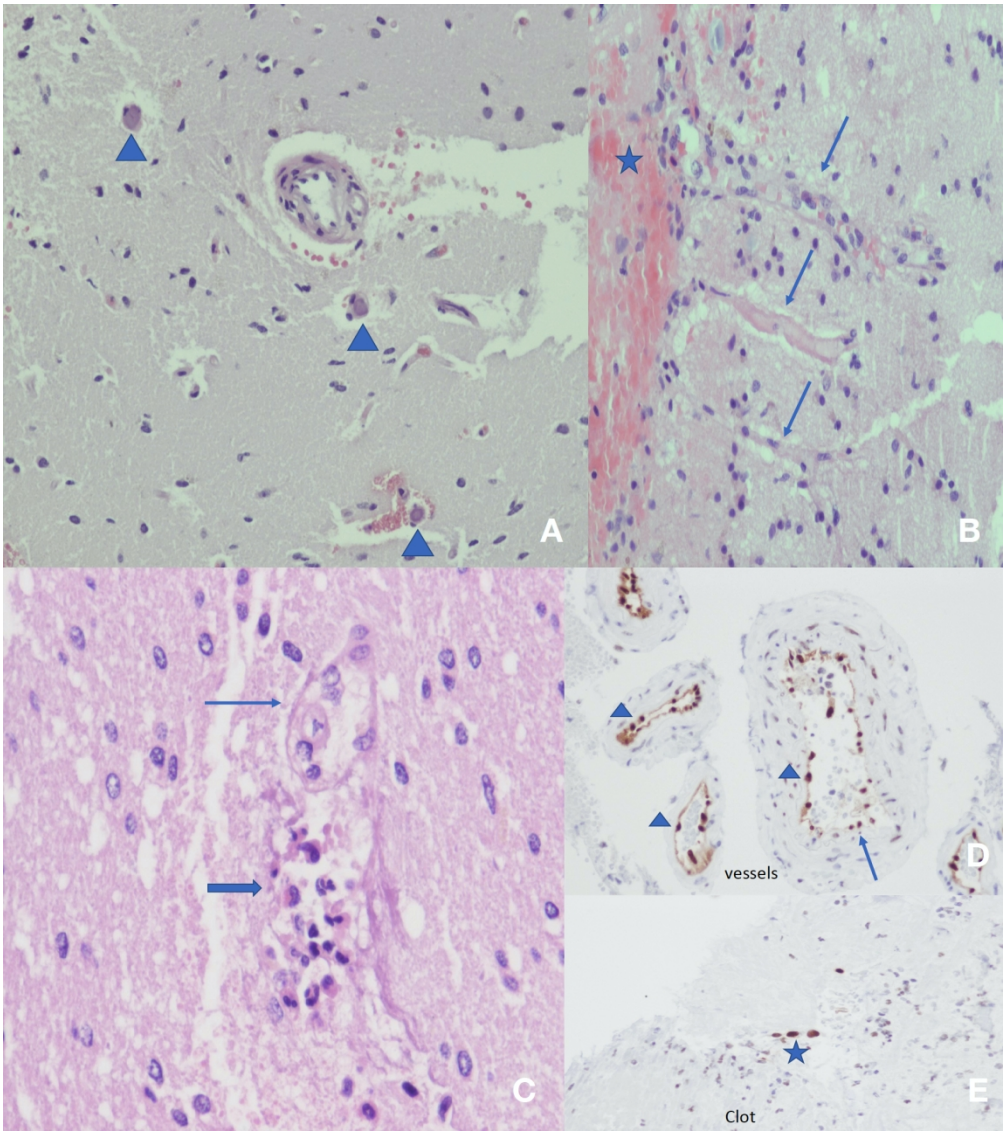

Figure 7. Patient 19 (A-D). Brain biopsy. HEx20 staining. A: Three microthrombi are observed (arrowhead). B: Image with 3 vessels (arrows): the upper one preserved with endothelial reactivity, intermediate vessel with preserved structure without viable cellularity. The lower one shows loss of endothelial cells. C: Capillary with evident alteration of endothelial cells and loss of adhesion (fine arrow). Extravasation of inflammatory cells with atypical lymphocytes in the perivascular space. D: Image of arteries and arterioles with reactive endothelial cells (arrowhead), some in the vessel lumen (small arrow) and normal endothelium (large arrow). E: Patient 3. Thrombotic material from a MT. Some endothelial cells (star) are observed.

159x179mm (300 x 300 DPI)